iScience

CellPress
OPEN ACCESS

Article

Contactless ultrasound spectroscopy for testing state-of-charge and integrity in lithium-ion batteries

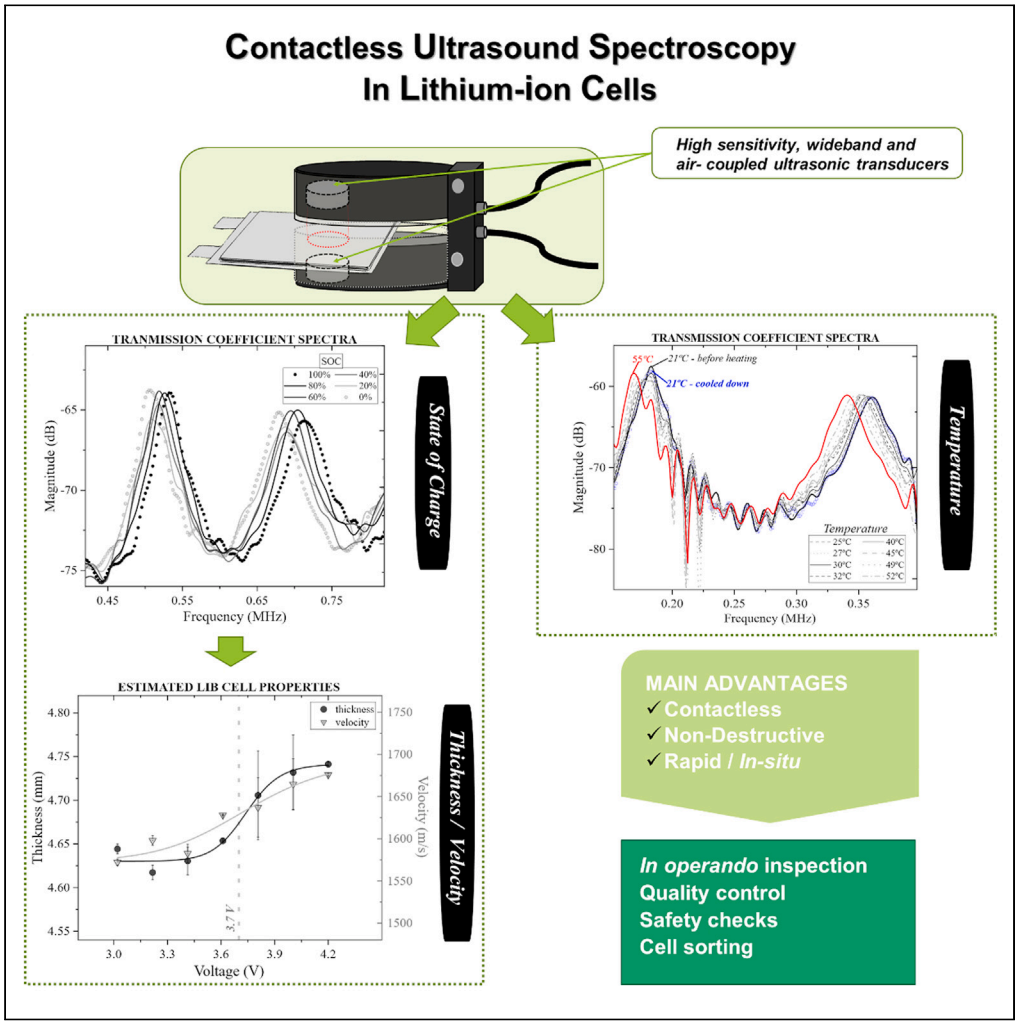

Lola Fariñas,
Manuel Muñoz,
Tomás E. Gómez
Álvarez-Arenas

lola.farinas@deusto.es

Highlights

A non-contact ultrasound spectroscopy technique enables testing of LIBs

Tested commercial cells showed repeatable thickness resonance trends during cycling

This technique estimates the thickness and the elastic modulus of LIBs in operando

Technique shows potential for early prediction of failures due to integrity issues

Fariñas et al., iScience 27, 111046
October 18, 2024
https://doi.org/10.1016/j.isci.2024.111046

iScience

CellPress
OPEN ACCESS

Article

Contactless ultrasound spectroscopy for testing state-of-charge and integrity in lithium-ion batteries

Lola Fariñas,[1,2,*] Manuel Muñoz,[1] and Tomás E. Gómez Álvarez-Arenas[1]

SUMMARY

Lithium-ion batteries (LIBs) are playing nowadays a key role in the decarbonization of the economy. However, safety issues and the lack of an accurate performance predictor after manufacturing led to the application of non-destructive methods in this field that can assess their condition. Contact ultrasounds have been successfully applied in recent years in this regard, mainly in research facilities, proving the potential of ultrasonic waves to collect meaningful information. However, some restrictions on their applicability have been identified, compromising their repeatability and stability in operando and in fabrication. Here, we present a contactless ultrasound spectroscopy technique based on the use of air-coupled transducers of high sensitivity and wide frequency band to detect state-of-charge (SOC)-related changes in LIB cells in operando. Additionally, its ability to detect mechanical integrity alterations was also revealed, showing the potential of contactless ultrasound spectroscopy as a powerful tool to test and predict early failures in LIBs.

INTRODUCTION

In the last decades, batteries have been incorporated into many sectors with huge economic impact, such as consumer electronics, electric mobility, or large-scale energy storage.[1,2] As of today, lithium-ion batteries (LIBs) lead this market and are expected to maintain this position in the near future. The main reasons that push LIBs to the forefront of energy storage technologies are their high energy density, long cycle life, high power output, low self-discharge, and safety, among others. However, the abrupt and growing demand has led to a rapid and steady development in the battery sector, where production, control, and research players have identified different needs along the value chain that are being pursued.[3] Some of these relate to in-line quality control at different stages,[4] including raw material testing,[5–7] end-of-line inspection of assembled cells,[4] and manufacturing optimization,[8,9] whereas others concern the monitoring of batteries in use[10] or end-of-life sorting for recycling/second use.[11] In parallel, the research sector is demanding alternative technologies that can help in the development of the new generation of battery cells and *in operando* techniques that facilitate their work, such as in postmortem analysis, state-of-health (SOH) and state-of-charge (SOC) monitoring, or early failure prediction.[12,13]

On the one hand, some of the techniques used for the aforementioned needs present challenges in terms of being destructive or difficult to deploy due to lack of speed, ease of inspection, or safety. On the other hand, more recently, techniques widely used in the non-destructive testing (NDT) sector have been applied in the inspection of LIBs. In this context, ultrasonic waves have been proven to be useful for the evaluation of SOC,[14–16] electrolyte wetting,[17] and defect detection,[18] among others, related to SOH assessment.[19,20] Interestingly, the information provided by ultrasonic methods, besides being convenient for the inspection of LIBs, is also highly valuable toward the understanding of their mechanical behavior.[21,22] However, a key issue in this regard is that LIBs are not only mechanically but also dimensionally dynamic: electrochemical operation leads to an inherent evolution of internal stresses and significant volume alterations.[23–25] Consequently, widely used ultrasonic methods based on contact techniques represent a major drawback for these purposes, as they are intrinsically quite sensitive to the pressure between the cell and the sensors, which directly affects the complexity of the measurement procedure, may modify the battery cell itself, and lacks of reproducibility and accuracy.

Non-contact ultrasound overcomes the mentioned weaknesses of contact techniques. Within the contactless ultrasound category, air-coupled ultrasound is preferred, as it is safer due to its low energy and more precise given its higher signal-to-noise ratio, as opposed to other techniques such as laser generation, which can present safety problems.[26] Although other limitations in air-coupled ultrasound were pointed out in previous attempts,[27,28] the use of efficient air-coupled ultrasonic transducers optimized for broadband and high-sensitivity applications is crucial to unlock the full potential of these contactless methods in battery cells.[29,30]

[1]Ultrasonic and Sensors Technologies Department (ITEFI), Spanish National Research Council (CSIC), 28006 Madrid, Spain
[2]Lead contact
*Correspondence: lola.farinas@deusto.es
https://doi.org/10.1016/j.isci.2024.111046

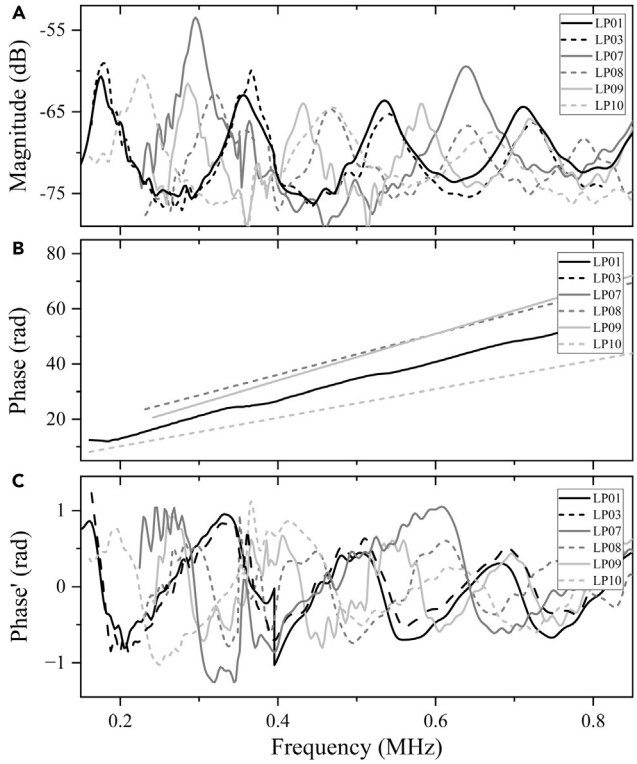

Figure 1. Ultrasonic transmission coefficient spectra of various LIBs

(A) Magnitude, (B) phase, and (C) rectified phase in which the effect of the resonances is highlighted for the sake of clarity. All spectra were measured at full charge.

In this work, we proposed a new method to characterize and test lithium-ion battery cells based on the use of non-contact ultrasound spectroscopy. We tested several commercial cells of different capacities and dimensions from two different manufacturers. Transmission coefficient spectra measured show characteristic thickness resonances that follow repeatable trends synchronized with electrochemical cycling in operando. From these ultrasonic experimental data, we directly determined effective properties of the LIBs *in situ*, such as the thickness, the ultrasonic velocity, and, hence, the elastic modules, the accuracy of which was verified by comparison with independent data. The results obtained position this technique as a great candidate to facilitate the study of the mechano-electro-chemical (MEC) behavior of batteries.[31–33] Finally, the potential of non-contact ultrasound spectroscopy for enabling early failure prediction due to mechanical integrity issues was evaluated.

RESULTS AND DISCUSSION

Air-coupled ultrasound spectroscopy for testing lithium-ion battery cells

The resonant ultrasound spectroscopy[34] is a technique used to evaluate the acoustic properties of a plate immersed in a fluid. In particular, considering a single-layered plate surrounded by air where a plane wave is normally incident to the plate, the transmitted coefficient spectra (T) can be obtained as:

$$T = \frac{2Z_aZ_s}{2Z_aZ_s\cos(kd)+i\left(Z_a^2+Z_s^2\right)\sin(kd)} \quad \text{(Equation 1)}$$

where Z_a and Z_s are the acoustic impedance of air and the plate sample, respectively, calculated as the product of density and ultrasonic propagation velocity; k is the wavenumber of the longitudinal wave in the plate; and d is the thickness.

In the particular case of this work, LIB is a complex multilayered material comprising a large number of alternating layers of anodes, cathodes, separators, etc. However, the individual thickness of each of these layers is several orders of magnitude smaller than the ultrasonic wavelength. Therefore, it is acceptable to assume an effective medium approach for the battery cell.

Figure 1 shows the transmitted spectra (T), depicting both magnitude and phase, of different LIB samples (see Table 2) tested in this study under constant voltage (100% SOC). Clear patterns revealing up to four peaks of thickness resonances within the experimental frequency range are shown. Hence, the observation of thickness resonances confirms the adequacy of the initially stated effective medium approach.

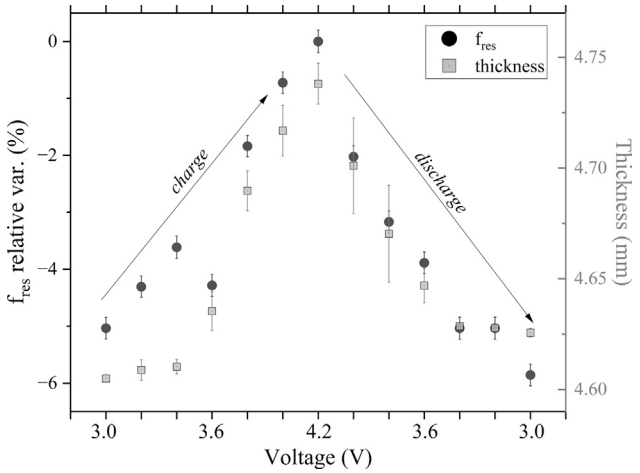

Figure 2. Evolution of thickness and relative variation in resonant frequency during electrochemical cycling in a LIB

Measurements were collected over four charge/discharge cycles, sampled every 0.2 V on cell LP01. Data are presented as mean ± SD.

That is, the T is dependent on the acoustic longitudinal wave properties, velocity, and attenuation of the whole battery that, in its turn, is the result of the different component layers within the LIB and the mechanical integrity and compaction of the entire cell.

Furthermore, as the resonance peaks observed in magnitude spectra correspond to the onset of constructive interferences of the ultrasonic field within the battery, they appear when wavelength equals two times the battery thickness and its multiples. Therefore, in the absence of attenuation, position of these resonance peaks can be obtained as[35]:

$$f_n = \frac{nv}{2d} \quad \text{(Equation 2)}$$

where f is the frequency at which the *n-th* thickness resonance maximum appears; v is the effective ultrasonic velocity through the sample; and d its total thickness. Figure 1 shows the particular ultrasonic response—*an acoustic fingerprint*—as consequence of its effective properties. In this case, ultrasonic fingerprints for batteries in a range of nominal capacities from 850 to 3,600 mAh and from two different manufacturers have been presented (see Table 2).

State-of-Charge and trends in ultrasonic spectra

During charging and discharging, repeatable trends can be clearly observed in the LIBs ultrasonic response. This feature can be seen in Figure 2 that shows the evolution in both the thickness and the resonant frequency—expressed as relative variation—during four electrochemical cycles at a current rate of 0.5C. Thickness was measured independently with a micrometer as explained in the *Experimental Procedures* section, whereas the resonant frequency values were directly obtained from the measured coefficient spectra by averaging the resonant frequencies of the 2nd and 3rd peaks at each point, with the aim of avoiding any perturbation in their position as a consequence of the border effect at the limit of the working bandwidth of the transducers.

The patterns observed are synchronized with the electrochemical cycling as previously reported in literature using different ultrasonic techniques.[14,32,36] These data reveal a shift in the cell resonant frequency that can be directly correlated with the voltage and thus with SOC: as the cell is charged, the resonant frequency shift toward higher values and, conversely, when discharged, these resonance peaks shift toward lower frequency values (up to −5.8%). According to Equation 2, changes in the resonant frequency may be due to alterations in the thickness, velocity, or both. Though, it is known that, in general, this type of cells expands with increasing voltage and shrinks with decreasing charge (effect known as cell *"breathing"*),[37,38] as it can be appreciated on the thickness mean values shown in Table 1. Consequently, in order to detect the measured frequency increment during charging, an increase in the effective ultrasonic velocity high enough to compensate the decrease in frequency caused by the expected thickening of the sample must be taking place. This effect is consistent with previous results reported in the literature using contact ultrasonic techniques.[14,32,39] Furthermore, the resonant frequency data during charging and discharging show a certain degree of asymmetry that can be consequence of the hysteretic behavior of the anodes.[40] In particular, at low currents, as in this case, the intercalation stages depend on whether the cell is being charged or discharged, and these differences are detectable using ultrasonic techniques.[41]

Figure 3 shows measured transmission coefficient spectra in several cells at different states of charge (only 100% and 0% SOC are plotted for the sake of clarity). In all cases, a shift toward higher frequencies in the spectra is observed when state-of-charge goes from 0% to 100%. This confirms the results in Figure 2; furthermore, this also suggests that this behavior is not solely attributable to a specific type of LIB but that it is rather general. In addition, it can be noticed that cycling influences not only the position of the maximum peaks in T magnitude but also the phase versus frequency slopes, supporting the already stated direct relationship between ultrasonic velocity and *state-of-charge* in LIBs.[30]

Table 1. Average effective properties of Lithium-ion battery cells

Sample	*State-of-charge*	Thickness ultrasound (mm)	Thickness micrometer (mm)	Velocity (m/s)	Elastic modulus (GPa)
LP01	100%	4.741 ± 0.002	4.752	1,676	7.61
LP01	0%	4.644 ± 0.006	4.606	1,572	6.83
LP03	100%	4.735 ± 0.032	4.727	1,688	7.75
LP03	0%	4.563 ± 0.016	4.602	1,549	6.77
LP07	100%	2.675 ± 0.110	2.691	1,581	5.62
LP07	0%	2.617 ± 0.328	2.616	1,495	5.14
LP08	100%	5.168 ± 0.074	5.168	1,635	6.81
LP08	0%	5.032 ± 0.054	5.044	1,515	6.00
LP09	100%	5.797 ± 0.040	5.844	1,696	7.21
LP09	0%	5.652 ± 0.016	5.684	1,553	6.20
LP10[a]	100%	3.615 ± 0.357	3.600	1,699	6.67
LP10[a]	0%	3.502 ± 0.392	3.529	1,646	6.47

[a]Anomalous measurements are not included (see corresponding section for further details).

Thickness resonances shifts and estimation of material properties

The technique proposed in this work, air-coupled resonant ultrasound spectroscopy, allows the evaluation of the effective acoustic longitudinal wave properties, including thickness, without the need of any additional measurement.[42] This feature can be particularly useful for *in situ* and *in operando* LIB characterization, representing an advantage compared to other methods[43] including contact and immersion ultrasonic techniques.[14,32,36]

Table 1 summarizes the mean experimental parameters measured at the maximum charge (100% SOC) and at the minimum recommended charge (0% SOC) in the LIBs studied in this work. In addition to the ultrasonic velocity and thickness, the macroscopic effective elastic modulus of each sample was estimated from the ultrasonic velocity (v) and volumetric density (ρ) (assuming only a thickness change with charge):[44]

$$M = v^2\rho \qquad \text{(Equation 3)}$$

Furthermore, independent thickness measurements obtained using a micrometer have been included in Table 1 for comparison purposes.

Comparing the ultrasonic and micrometer estimation of battery thickness, the relative variation is less than 0.85%. This fact supports the suitability of the contactless resonant ultrasound spectroscopy for battery cell effective thickness estimation. In this regard, we have utilized air data considering normal conditions; therefore, in order to fine-tune the results, the introduction of real-time measurements of air pressure, temperature, and humidity can be considered in the future. As for the micrometer method, the errors depend on the applied pressure and surface roughness, two factors that are difficult to avoid.

The maximum thickening as consequence of the SOC is between 2% and 3%, whereas ultrasonic velocity increases by 6%–8%. The elastic moduli of the cells at full charge are between 9% and 13% higher with the exception of LP10. These results agree with those obtained using different techniques in literature.[21,22,38] The standard deviation obtained for the LP07 sample is notably higher than the others. The transmission coefficient measured (Figure 3B) indicates a certain degree of coupling between the 2nd and 3rd peaks of resonances, which may be the cause of this difference. Future work will thoroughly investigate this behavior in samples whose composition is well known *a priori*.

In summary, data follow the expected trends: for battery cells, which are composed by different layers including electrodes and electrolyte-impregnated separators, it is well-known that the material properties of the electrodes change as consequence of electrochemical cycling.[45,46] In the particular case of pouch cells in which the described structure is weakly constrained by an aluminum foil, global thickness changes can be measured that are directly correlated with voltage,[38] as in the LIBs used in this work and supported by the results shown in Table 1. In the case of the elastic modulus, a feasible explanation is that as consequence of the thickening of some layers within the cells at high SOCs—mainly due to delithiation at different phase transitions of graphite[47] in the anode—the internal pressure increases by means of the stress caused by the thickening against the aluminum foil packaging. This would explain the elastic modulus variations measured by the ultrasonic technique at different SOCs.

Figure 4 shows the variation in the thickness and longitudinal ultrasonic velocity with voltage during discharge for samples LP01 and LP03, which correspond to identically manufactured cells according to their datasheet (see Table 2). The data collected from LP01 correspond to a higher number of cycles (from 4 to 12) than those of LP03 (up to 4). The thickness follows the expected trend, where it shrinks as the cell voltage decreases and expands at higher SOCs. In the case of velocity, it also decreases with voltage, as explained in previous section. Thus, the experimental data have been fitted to sigmoidal functions whose inflection point is located at 3.7 V, obtaining R^2 greater than 0.90 in all cases. The main differences between the two LIBs can be appreciated in the thicknesses for the lower states of charge (below the inflection point),

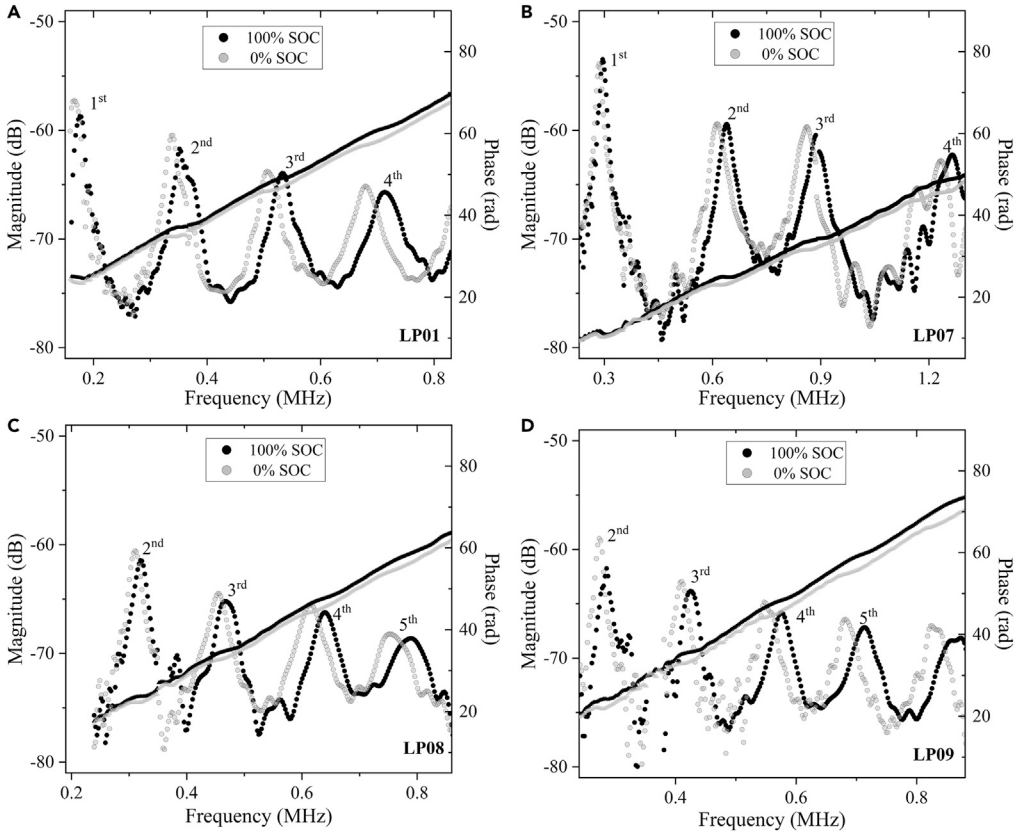

Figure 3. Variations in transmission coefficient spectra with State-of-Charge

Magnitude and phase of up to five thickness resonance peaks measured at 100% and 0% charge in four different LIBs: (A) LP01; (B) LP07; (C) LP08; (D) LP09.

when thinner values were obtained for the LP03. In terms of velocity, the range of variation is almost 2% higher for the LP03 cell, whose maximum velocity is greater than LP01. Consequently, LP03 elastic modulus is higher than LP01 (see Table 2). These detected changes, assuming identical initial materials and structure, can be attributed to differences on the density of the forming layers, the degree of compaction of the layered structure, or both. Knehr et al.[48] defined a *break-in* period characteristic of LCO/graphite pouch cells, where abrupt changes in the electrochemical impedance and ultrasonic signal take place, followed by a gradual stabilization toward constant values. This would explain the presented results since LP03 cell would correspond to the beginning of the *break-in* period while the LP01 would be situated at its very end, closer to the plateau. The described behavior was attributed to a stage in which the graphite anode grows, causing an increment of the thickness of the battery cell while the effective modulus decreases. This reduction of the modulus after an "excessive" increase of the thickness could be interpreted as a deterioration in the degree of compaction of the cell that implies the regular aging of LIBs.

Further work will be conducted to unravel the variation in estimated parameters due to manufacturing tolerances and the effect of other factors, such as cell cycling and failure. The latter is expected to contribute to the loss of compaction pressure in the cell that is expected when the thickening is too large and the deformation of the packaging materials is entering the plastic regime.

Temperature and trends in ultrasonic spectra

It is of interest to understand the effect of temperature on the ultrasonic spectra, especially with the motivation of being able to apply these techniques to *in operando* monitoring of cells including at high C-rates. To this end, a cell (LP01) was measured with the air-coupled ultrasonic technique at constant SOC at room temperature before being heated in the oven to 55°C. It was then let cool to room temperature while its coefficient spectra were measured. Figure 5A shows the evolution of the first and second resonance peaks during this experiment. A clear shift toward lower frequencies is observed reaching a relative variation of up to 2% higher than the maximum range measured between 100% and 0% SOC during cycling (see Figure 3). It is worth noting that although the resonance frequency and SOC maintain a direct relationship, for temperature the relationship found was inversed, reaching values close to the ones at 0% SOC at maximum temperature in the resonance peaks. In addition, the thicknesses were independently measured and no significant variation was obtained. Conversely, the thicknesses estimated using the ultrasonic technique showed an expansion of up to 2% at maximum temperature compared to its initial state (see Figure 5B). Regarding the resonant frequency, a maximum relative variation of −5.74% was detected at 55°C, indicating that other factors, among

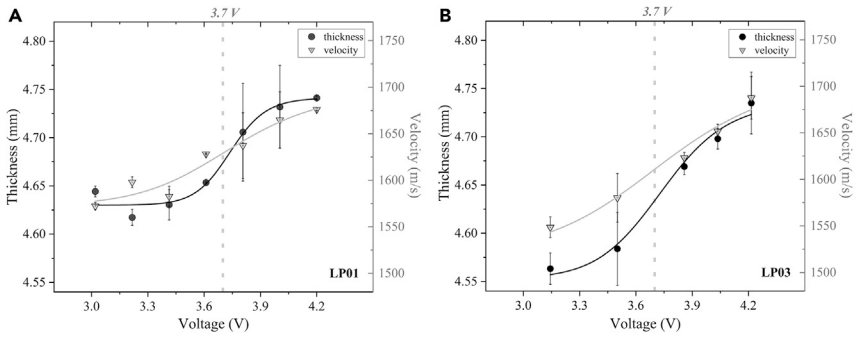

Figure 4. Evolution of thickness and ultrasonic velocity during discharge in two identically manufactured LIBs

A comparison between mean thickness (black circles) and velocitiy (gray triangles) directly estimated from ultrasonic measurements. Significant sigmoidal fittings with inflection points at 3.7 V for both parameters are shown (solid lines): (A) LP01; (B) LP03. Data are presented as mean ± SD.

thickening, were altered by the temperature increase in the cell, causing a diminution of the ultrasonic velocity and consequently on the elastic modulus as the density also decreases. These results are similar to those reported by Owen et al.[41] in which an increase in the *time-of-flight* measured by contact ultrasonic techniques was related to a decrease in ultrasonic velocity. This kind of behavior has been described in materials with elastic properties in the range of the LIBs components.[49] Upon cooling, a recovery of thickness and frequency was measured that did not follow a constant rate with temperature. Back at room temperature, the ultrasonic spectra measured is similar to the one taken at the beginning of the experiment; therefore, it should be noted that specially the estimated thickness was still 3% below its initial value. Together with material expansion, a change in electrolyte viscosity could explain this behavior, as it acts as a couplant throughout the cell playing a key role in effective mechanical cohesion. Hence, the steepest slope in the estimated parameter recovery with temperature was found outside the optimal LIB operating temperature window (20°C–40°C), where battery is expected to suffer accelerated aging.[50] Nonetheless, future experiments will be compared with complementary techniques for validation, since the possibility of measuring changes in LIBs as a consequence of temperature alterations and, more importantly, the possibility of decoupling their effects *in operando* have been enunciated as being of great interest in this field.[20]

Anomalous thickening and its influence on ultrasonic spectra

During the experimental tests performed for this work, the aforementioned repeated trends on the ultrasonic spectra during cycling have been a constant. However, the LP10 cell presented anomalous behavior compared to the rest. Although initially, a thickness resonant pattern in the ultrasonic transmission coefficient was measured as shown in the experimental transmission coefficient labeled as 1 in Figure 6A (for wider spectra, see Figure 1), in a subsequent test, a strong loss of acoustic signal was detected (transmission coefficient labeled as 2 in Figure 6A). After 36 h at rest, the thickness resonances were clearly observed back again enabling a new complete loading/unloading experiment (some of these measurements are labeled corresponding to spectra from 3 to 8 in Figure 6A). Finally, for the next cycling experiment, the resonances disappeared definitely (labels beyond 8). In parallel to the non-contact ultrasonic spectroscopy measurements, thicknesses were obtained independently in the same cell and collected in Figure 6B. The lack of resonance detection is coincident with an uncommon thickening of the cell reaching values higher than 3.70 mm on average, which represents a relative variation of more than double in percentage than that registered for other cells of the same manufacturer according to Table 2. Cell swelling as a result of gassing is not uncommon in faulty LIBs, whose effects include increase in cell stress leading to cell cracking[19,51] and delaminations.[52] In this regard, the detected drastic loss of ultrasonic signal and a spontaneous recovery can be strong evidence of gassing inside the cell,[53] which was identified as an early sign of thermal runaway and failure, as it occurs before other significant rates are recorded.[20]

Figure 6C presents the nominal capacity and mean elastic modulus values measured at 100% and 0% SOC for each type of LIB considered in this work. As shown, a significant linear fit correlates nominal capacity and elastic modulus at both charge states. However, further

Table 2. Lithium-ion polymer battery cell samples

Sample	Description	Capacity (mAh)	Dimensions (mm)	Density (kg/m^3)
LP01	NIMO LP486684	3,600	76.00 × 63.50 × 4.65	2,758
LP03	NIMO LP486684	3,600	76.00 × 63.50 × 4.65	2,763
LP07	CELLEVIA LP294862	850	60.00 × 50.00 × 2.64	2,290
LP08	CELLEVIA L584174	1,800	65.00 × 41.00 × 5.10	2,575
LP09	CELLEVIA L654290	2,600	89.00 × 40.00 × 5.75	2,528
LP10	CELLEVIA LP405090	1,800	90.00 × 52.00 × 3.70	2,316

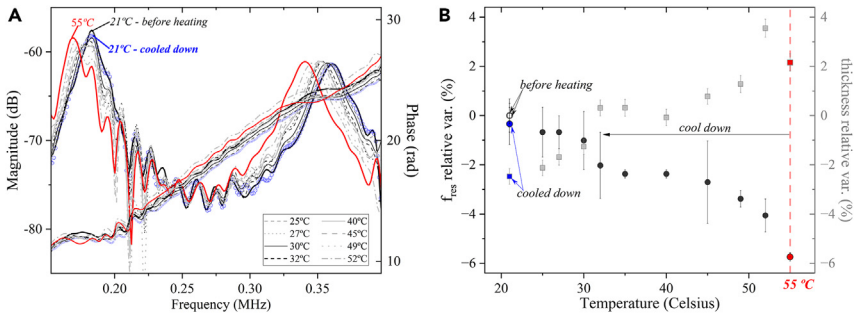

Figure 5. Ultrasonic changes with temperature variation

(A) Transmission coefficient spectra measured during the cooling of an LP01 cell after heating to 55°C.

(B) Relative variations in resonant frequency (black circles) and thickness (gray squares) during the cooling of the LP01 cell. Data are presented as mean ± SD.

information on cell layer composition is not available, preventing a more thorough understanding of this relationship. Nonetheless, it should be noted that the LP10 cell, considering the values obtained from cycling measurements where thickness resonances were present, shows an acute deviation at 0% SOC toward higher values. Consequently, the range of relative variation between both charge states represented is less than half compared to the rest of samples (see Table 1). A feasible explanation to this behavior matches with the aforementioned gassing, which was reported to increase the internal stresses in the cell due to mechanical constraints.[25]

In this regard, the presented technique would shed light by disentangling the effects of volume-pressure change and gassing, which represents a technical issue with some current detection methods.[48,54] Future work will systematically study the effect of phenomena such as gassing and delamination using non-contact ultrasonic spectroscopy to evaluate the performance of these techniques as early predictor of integrity and *state-of-health* issues in battery cells.

Conclusions

This work demonstrates that it is possible to measure, at normal incidence, transmission coefficient spectra in lithium-ion pouch cells of different sizes and capacities using presently available electronics and wideband and high-sensitivity air-coupled ultrasonic transducers with excellent SNR. Spectral analysis of the transmission coefficients reveals that it is possible to excite and sense thickness resonances that exhibit repeatable trends synchronized with the electrochemical cycling. Analysis of these resonances permit to extract thickness, velocity, and elastic modulus in the cell without any *a priori* information. The presented results show that the contactless ultrasound spectroscopy enables non-destructive, rapid, and *in situ* estimation of the effective battery cell parameters with sufficient accuracy to detect changes mainly driven by electrochemical stiffness and compaction degree taken *in operando*. Finally, contactless ultrasound spectroscopy was found to reveal alterations due to induced temperature changes as well as anomalous cell behavior, unveiling the potential of the proposed technique to be used as an early predictor of batteries failure.

Limitations of the study

In this work, we mainly focused on the feasibility of applying contactless ultrasound for the study of lithium-ion pouch cells, as well as on the excitation and sensing of thickness resonances, which allow for the rapid and non-invasive estimation of parameters such as ultrasound velocity, thickness, or elastic modulus *in situ*. However, no detailed information about the chemistries, composition, or electrochemical performance was obtained from the commercial suppliers, who were not the manufacturers. In future work, it will be valuable to further investigate the impact of cell chemistries on the acoustic fingerprint measured using air-coupled ultrasound.

RESOURCE AVAILABILITY

Lead contact

Further information should be directed to and will be fulfilled by the lead contact, Lola Fariñas (lola.farinas@deusto.es).

Materials availability

This study did not generate new unique materials.

Data and code availability

- The data reported in this paper will be shared by the lead contact upon request.
- This paper does not report original code.
- Any additional information required to reanalyze the data reported in this paper is available from the lead contact upon request.

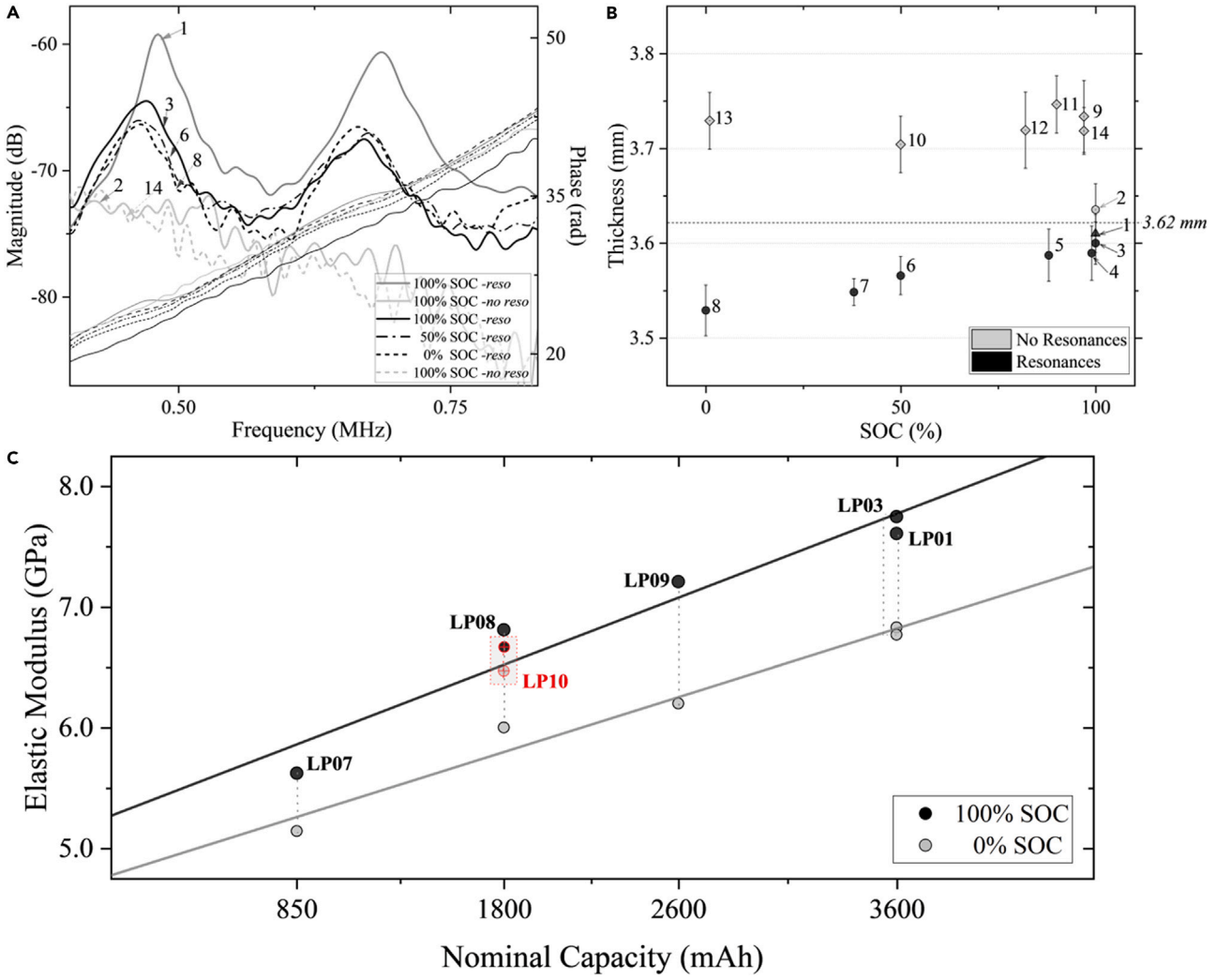

Figure 6. Anomalous thickening and disappearance of thickness resonances

(A) Transmission coefficient spectra of LP10 obtained during cycling tests.

(B) Thickness measurements of LP10 across different cycling tests. Data are represented as mean ± SD.

(C) Comparison of nominal capacity with the mean elastic modulus measured in all LIB samples.

ACKNOWLEDGMENTS

Financial support through fellowship Juan de la Cierva - incorporación (JC2020-043487-I) funded by MCIN/AEI/10.13039/501100011033 and by "European Union NextGenerationEU/PRTR" is acknowledged.

AUTHOR CONTRIBUTIONS

Conceptualization, L.F, M.M., and T.G.; methodology, L.F., M.M., and T.G.; investigation, L.F. and T.G.; writing—original draft, L.F.; writing—review & editing, M.M. and T.G.; funding acquisition, L.F. and T.G.

DECLARATION OF INTERESTS

The authors declare no competing interests.

STAR★METHODS

Detailed methods are provided in the online version of this paper and include the following:

- KEY RESOURCES TABLE
- METHOD DETAILS

Received: May 29, 2024
Revised: July 30, 2024
Accepted: September 23, 2024
Published: September 26, 2024

REFERENCES

1. Faunce, T.A., Prest, J., Su, D., Hearne, S.J., and Iacopi, F. (2018). On-grid batteries for large-scale energy storage: Challenges and opportunities for policy and technology. MRS Energy Sustain. *5*, 10. https://doi.org/10.1557/mre.2018.11.
2. Ding, Y., Cano, Z.P., Yu, A., Lu, J., and Chen, Z. (2019). Automotive Li-Ion Batteries: Current Status and Future Perspectives. Electrochem. Energy Rev. *2*, 1–28. https://doi.org/10.1007/s41918-018-0022-z.
3. Grant, P.S., Greenwood, D., Pardikar, K., Smith, R., Entwistle, T., Middlemiss, L.A., Murray, G., Cussen, S.A., Lain, M.J., Capener, M.J., et al. (2022). Roadmap on Li-ion battery manufacturing research. JPhys Energy *4*, 042006. https://doi.org/10.1088/2515-7655/ac8e30.
4. McGovern, M.E., Bruder, D.D., Huemiller, E.D., Rinker, T.J., Bracey, J.T., Sekol, R.C., and Abell, J.A. (2023). A review of research needs in nondestructive evaluation for quality verification in electric vehicle lithium-ion battery cell manufacturing. J. Power Sources *561*, 232742. https://doi.org/10.1016/j.jpowsour.2023.232742.
5. Mutz, M., Perovic, M., Gümbel, P., Steinbauer, V., Taranovskyy, A., Li, Y., Beran, L., Käfer, T., Dröder, K., Knoblauch, V., et al. (2022). Toward a Li-Ion Battery Ontology Covering Production and Material Structure. Energy Technol. *11*, 2200681. https://doi.org/10.1002/ente.202200681.
6. Grant, A., and O'Dwyer, C. (2023). Real-time nondestructive methods for examining battery electrode materials. Appl. Phys. Rev. *10*. https://doi.org/10.1063/5.0107386.
7. Zhang, Y.S., Pallipurath Radhakrishnan, A.N., Robinson, J.B., Owen, R.E., Tranter, T.G., Kendrick, E., Shearing, P.R., and Brett, D.J.L. (2021). *In Situ* Ultrasound Acoustic Measurement of the Lithium-Ion Battery Electrode Drying Process. ACS Appl. Mater. Interfaces *13*, 36605–36620. https://doi.org/10.1021/acsami.1c10472.
8. Ayerbe, E., Berecibar, M., Clark, S., Franco, A.A., and Ruhland, J. (2022). Digitalization of Battery Manufacturing: Current Status, Challenges, and Opportunities. Adv. Energy Mater. *12*, 2102696. https://doi.org/10.1002/aenm.202102696.
9. Weng, A., Mohtat, P., Attia, P.M., Sulzer, V., Lee, S., Less, G., and Stefanopoulou, A. (2021). Predicting the impact of formation protocols on battery lifetime immediately after manufacturing. Joule *5*, 2971–2992. https://doi.org/10.1016/j.joule.2021.09.015.
10. Wei, Z., Zhao, J., He, H., Ding, G., Cui, H., and Liu, L. (2021). Future smart battery and management: Advanced sensing from external to embedded multi-dimensional measurement. J. Power Sources *489*, 229462. https://doi.org/10.1016/j.jpowsour.2021.229462.
11. Mishra, G., Jha, R., Meshram, A., and Singh, K.K. (2022). A review on recycling of lithium-ion batteries to recover critical metals. J. Environ. Chem. Eng. *10*, 108534. https://doi.org/10.1016/j.jece.2022.108534.
12. Pradhan, S.K., and Chakraborty, B. (2022). Battery management strategies: An essential review for battery state of health monitoring techniques. J. Energy Storage *51*, 104427. https://doi.org/10.1016/j.est.2022.104427.
13. Sulzer, V., Mohtat, P., Aitio, A., Lee, S., Yeh, Y.T., Steinbacher, F., Khan, M.U., Lee, J.W., Siegel, J.B., Stefanopoulou, A.G., and Howey, D.A. (2021). The challenge and opportunity of battery lifetime prediction from field data. Joule *5*, 1934–1955. https://doi.org/10.1016/j.joule.2021.06.005.
14. Hsieh, A.G., Bhadra, S., Hertzberg, B.J., Gjeltema, P.J., Goy, A., Fleischer, J.W., and Steingart, D.A. (2015). Electrochemical-acoustic time of flight: in operando correlation of physical dynamics with battery charge and health. Energy Environ. Sci. *8*, 1569–1577. https://doi.org/10.1039/C5EE00111K.
15. Davies, G., Knehr, K.W., Van Tassell, B., Hodson, T., Biswas, S., Hsieh, A.G., and Steingart, D.A. (2017). State of Charge and State of Health Estimation Using Electrochemical Acoustic Time of Flight Analysis. J. Electrochem. Soc. *164*, A2746–A2755. https://doi.org/10.1149/2.1411712jes.
16. Meng, K., Chen, X., Zhang, W., Chang, W., and Xu, J. (2022). A robust ultrasonic characterization methodology for lithium-ion batteries on frequency-domain damping analysis. J. Power Sources *547*, 232003. https://doi.org/10.1016/j.jpowsour.2022.232003.
17. Deng, Z., Huang, Z., Shen, Y., Huang, Y., Ding, H., Luscombe, A., Johnson, M., Harlow, J.E., Gauthier, R., and Dahn, J.R. (2020). Ultrasonic Scanning to Observe Wetting and "Unwetting" in Li-Ion Pouch Cells. Joule *4*, 2017–2029. https://doi.org/10.1016/j.joule.2020.07.014.
18. Robinson, J.B., Owen, R.E., Kok, M.D.R., Maier, M., Majasan, J., Braglia, M., Stocker, R., Amietszajew, T., Roberts, A.J., Bhagat, R., et al. (2020). Identifying Defects in Li-Ion Cells Using Ultrasound Acoustic Measurements. J. Electrochem. Soc. *167*, 120530. https://doi.org/10.1149/1945-7111/abb174.
19. Robinson, J.B., Pham, M., Kok, M.D., Heenan, T.M., Brett, D.J., and Shearing, P.R. (2019). Examining the Cycling Behaviour of Li-Ion Batteries Using Ultrasonic Time-of-Flight Measurements. J. Power Sources *444*, 227318. https://doi.org/10.1016/j.jpowsour.2019.227318.
20. Williams, D., Copley, R., Bugryniec, P., Dwyer-Joyce, R., and Brown, S. (2024). A review of ultrasonic monitoring: Assessing current approaches to Li-ion battery monitoring and their relevance to thermal runaway. J. Power Sources *590*, 233777. https://doi.org/10.1016/j.jpowsour.2023.233777.
21. Chang, W., Mohr, R., Kim, A., Raj, A., Davies, G., Denner, K., Park, J.H., and Steingart, D. (2020). Measuring effective stiffness of Li-ion batteries *via* acoustic signal processing. J. Mater. Chem. A Mater. *8*, 16624–16635. https://doi.org/10.1039/D0TA05552B.
22. Feiler, S., Daubinger, P., Gold, L., Hartmann, S., and Giffin, G.A. (2023). Interplay between Elastic and Electrochemical Properties during Active Material Transitions and Aging of a Lithium-Ion Battery. Batter. Supercaps *6*, e202200518. https://doi.org/10.1002/batt.202200518.
23. Jin, C., Wang, Y., Borujerdi, A.S., and Li, J. (2022). Stress evolution and thickness change of a lithium-ion pouch cell under various cycling conditions. J. Power Sources Adv. *16*, 100103. https://doi.org/10.1016/j.powera.2022.100103.
24. Lee, J.H., Lee, H.M., and Ahn, S. (2003). Battery dimensional changes occurring during charge/discharge cycles—thin rectangular lithium ion and polymer cells. J. Power Sources *119–121*, 833–837. https://doi.org/10.1016/S0378-7753(03)00281-7.
25. Li, R., Li, W., Singh, A., Ren, D., Hou, Z., and Ouyang, M. (2022). Effect of external pressure and internal stress on battery performance and lifespan. Energy Storage Mater. *52*, 395–429. https://doi.org/10.1016/j.ensm.2022.07.034.
26. Sampath, S., Yin, X., Tham, Z.W., Chen, Y.F., and Zhang, L. (2024). Real-time and non-contact estimation of state of charge for lithium-ion battery using laser ultrasonics. J. Power Sources *605*, 234544. https://doi.org/10.1016/j.jpowsour.2024.234544.
27. Chang, J.-J., Zeng, X.-F., and Wan, T.-L. (2019). Real-time measurement of lithium-ion batteries' state-of-charge based on air-coupled ultrasound. AIP Adv. *9*, 085116. https://doi.org/10.1063/1.5108873.
28. Cho, H., Kil, E., Jang, J., Kang, J., Song, I., and Yoo, Y. (2022). Air-Coupled Ultrasound Sealing Integrity Inspection Using Leaky Lamb Waves in a Simplified Model of a Lithium-Ion Pouch Battery: Feasibility Study. Sensors *22*, 6718. https://doi.org/10.3390/s22176718.
29. Gomez Alvarez-Arenas, T.E., Shrout, T.R., Zhang, S.J., and Lee, H.J. (2012). Air-Coupled Transducers Based on 1-3 Connectivity Single Crystal Piezocomposites. In 2012 IEEE International Ultrasonics Symposium (IEEE) (IEEE), pp. 2230–2233. https://doi.org/10.1109/ULTSYM.2012.0557.

30. Fariñas, L., Sánchez, M.M., and Álvarez-Arenas, T.G. (2023). Lithium-Ion Batteries' State-Of-Charge and Health Assessment by Non-Contact Ultrasound Spectroscopy. In 2023 IEEE International Ultrasonics Symposium (IUS) (IEEE) (IEEE), pp. 1–4. https://doi.org/10.1109/IUS51837.2023.10306820.
31. Nicholas, J.D., Qi, Y., Bishop, S.R., and Mukherjee, P.P. (2014). Introduction to Mechano-Electro-Chemical Coupling in Energy Related Materials and Devices. J. Electrochem. Soc. *161*, Y11–Y12. https://doi.org/10.1149/2.0231411jes.
32. Ladpli, P., Kopsaftopoulos, F., and Chang, F.-K. (2018). Estimating state of charge and health of lithium-ion batteries with guided waves using built-in piezoelectric sensors/actuators. J. Power Sources *384*, 342–354. https://doi.org/10.1016/j.jpowsour.2018.02.056.
33. Wang, M.J., Kazyak, E., Dasgupta, N.P., and Sakamoto, J. (2021). Transitioning solid-state batteries from lab to market: Linking electro-chemo-mechanics with practical considerations. Joule *5*, 1371–1390. https://doi.org/10.1016/j.joule.2021.04.001.
34. Schindel, D.W., and Hutchins, D.A. (1995). Through-thickness characterization of solids by wideband air-coupled ultrasound. Ultrasonics *33*, 11–17. https://doi.org/10.1016/0041-624X(95)00011-Q.
35. Truell, R., Elbaum, C., and Chick, B.B. (1969). Ultrasonic Methods in Solid State Physics (Academic Press).
36. Gold, L., Bach, T., Virsik, W., Schmitt, A., Müller, J., Staab, T.E., and Sextl, G. (2017). Probing lithium-ion batteries' state-of-charge using ultrasonic transmission – Concept and laboratory testing. J. Power Sources *343*, 536–544. https://doi.org/10.1016/j.jpowsour.2017.01.090.
37. Wang, X., Sone, Y., Segami, G., Naito, H., Yamada, C., and Kibe, K. (2007). Understanding Volume Change in Lithium-Ion Cells during Charging and Discharging Using In Situ Measurements. J. Electrochem. Soc. *154*, A14. https://doi.org/10.1149/1.2386933.
38. Rieger, B., Schlueter, S., Erhard, S.V., Schmalz, J., Reinhart, G., and Jossen, A. (2016). Multi-scale investigation of thickness changes in a commercial pouch type lithium-ion battery. J. Energy Storage *6*, 213–221. https://doi.org/10.1016/j.est.2016.01.006.
39. Zhang, B., Lyu, Y., Gao, J., Song, G., Zheng, Y., Lee, Y., and He, C. (2023). Ultrasonic characterization of multi-layered porous lithium-ion battery structure for state of charge. Ultrasonics *134*, 107060. https://doi.org/10.1016/j.ultras.2023.107060.
40. Grimsmann, F., Brauchle, F., Gerbert, T., Gruhle, A., Knipper, M., and Parisi, J. (2017). Hysteresis and current dependence of the thickness change of lithium-ion cells with graphite anode. J. Energy Storage *12*, 132–137. https://doi.org/10.1016/j.est.2017.04.006.
41. Owen, R.E., Robinson, J.B., Weaving, J.S., Pham, M.T.M., Tranter, T.G., Neville, T.P., Billson, D., Braglia, M., Stocker, R., Tidblad, A.A., et al. (2022). Operando Ultrasonic Monitoring of Lithium-Ion Battery Temperature and Behaviour at Different Cycling Rates and under Drive Cycle Conditions. J. Electrochem. Soc. *169*, 040563. https://doi.org/10.1149/1945-7111/ac6833.
42. Álvarez-Arenas, T.E.G. (2010). Simultaneous determination of the ultrasound velocity and the thickness of solid plates from the analysis of thickness resonances using air-coupled ultrasound. Ultrasonics *50*, 104–109. https://doi.org/10.1016/j.ultras.2009.09.009.
43. Piller, S., Perrin, M., and Jossen, A. (2001). Methods for state-of-charge determination and their applications. J. Power Sources *96*, 113–120. https://doi.org/10.1016/S0378-7753(01)00560-2.
44. Auld, B.A. (1990). Acoustic Fields and Waves in Solids, 2nd ed. (Krieger Publishing Company).
45. Qi, Y., Guo, H., Hector, L.G., and Timmons, A. (2010). Threefold Increase in the Young's Modulus of Graphite Negative Electrode during Lithium Intercalation. J. Electrochem. Soc. *157*, A558. https://doi.org/10.1149/1.3327913.
46. Pondick, J.V., Yazdani, S., Yarali, M., Reed, S.N., Hynek, D.J., and Cha, J.J. (2021). The Effect of Mechanical Strain on Lithium Staging in Graphene. Adv. Electron. Mater. *7*, 2000981. https://doi.org/10.1002/aelm.202000981.
47. Tavassol, H., Jones, E.M.C., Sottos, N.R., and Gewirth, A.A. (2016). Electrochemical stiffness in lithium-ion batteries. Nat. Mater. *15*, 1182–1187. https://doi.org/10.1038/nmat4708.
48. Knehr, K.W., Hodson, T., Bommier, C., Davies, G., Kim, A., and Steingart, D.A. (2018). Understanding Full-Cell Evolution and Non-chemical Electrode Crosstalk of Li-Ion Batteries. Joule *2*, 1146–1159. https://doi.org/10.1016/j.joule.2018.03.016.
49. Nowacki, K., and Kasprzyk, W. (2010). The Sound Velocity in an Alloy Steel at High-Temperature Conditions. Int. J. Thermophys. *31*, 103–112. https://doi.org/10.1007/s10765-009-0683-2.
50. Zappen, H., Fuchs, G., Gitis, A., and Sauer, D. (2020). In-Operando Impedance Spectroscopy and Ultrasonic Measurements during High-Temperature Abuse Experiments on Lithium-Ion Batteries. Batteries *6*, 25. https://doi.org/10.3390/batteries6020025.
51. Oca, L., Guillet, N., Tessard, R., and Iraola, U. (2019). Lithium-ion capacitor safety assessment under electrical abuse tests based on ultrasound characterization and cell opening. J. Energy Storage *23*, 29–36. https://doi.org/10.1016/j.est.2019.02.033.
52. Pham, M.T., Darst, J.J., Finegan, D.P., Robinson, J.B., Heenan, T.M., Kok, M.D., Iacoviello, F., Owen, R., Walker, W.Q., Magdysyuk, O.V., et al. (2020). Correlative acoustic time-of-flight spectroscopy and X-ray imaging to investigate gas-induced delamination in lithium-ion pouch cells during thermal runaway. J. Power Sources *470*, 228039. https://doi.org/10.1016/j.jpowsour.2020.228039.
53. Bommier, C., Chang, W., Li, J., Biswas, S., Davies, G., Nanda, J., and Steingart, D. (2020). Operando Acoustic Monitoring of SEI Formation and Long-Term Cycling in NMC/SiGr Composite Pouch Cells. J. Electrochem. Soc. *167*, 020517. https://doi.org/10.1149/1945-7111/ab68d6.
54. Louli, A.J., Ellis, L.D., and Dahn, J.R. (2019). Operando Pressure Measurements Reveal Solid Electrolyte Interphase Growth to Rank Li-Ion Cell Performance. Joule *3*, 745–761. https://doi.org/10.1016/j.joule.2018.12.009.

STAR★METHODS

KEY RESOURCES TABLE

REAGENT or RESOURCE	SOURCE	IDENTIFIER
Other		
Pouch cell – 3600 mAh	NIMO LP486684	https://www.electronicaembajadores.com/
Pouch cell – 850 mAh	CELLEVIA LP294862	https://www.tme.eu/
Pouch cell – 1800 mAh	CELLEVIA L584174	https://www.tme.eu/
Pouch cell – 2600 mAh	CELLEVIA L654290	https://www.tme.eu/
Pouch cell – 1800 mAh	CELLEVIA LP405090	https://www.tme.eu/
Olympus 5058PR	Olympus	https://www.olympus-ims.com/
Tektronix DPO7054	Tektronix	https://www.tek.com/
Velleman VLE8	Velleman	https://www.velleman.eu/
Mitutoyo micrometer ±0.01 mm	Mitutoyo	https://shop.mitutoyo.eu/

METHOD DETAILS

Cell samples

Six different samples from five different models of pouch-type lithium-ion polymer cells were bought from two commercial manufacturers (see Table 2).

Non-contact ultrasound spectroscopy

Air-coupled ultrasonic transducers

Three pairs of high sensitivity and wide band air-coupled ultrasonic piezoelectric transducers designed and built at CSIC lab were used (see below table).

Air-coupled transducers specifications			
Center Frequency (MHz)	Peak Sensitivity (dB)	Frequency Band (MHz)	Radiating Surface Diameter (mm)
0.25	−25	0.13–0.36	25
0.65	−30	0.35–0.95	20
1.00	−32	0.65–1.60	15

Ultrasonic equipment

A commercial pulser/receiver (5058PR, Olympus, TX, USA) was used for all the ultrasonic measurements. This pulser provides a spike of 900 V to drive the transmitter transducer. The cutoff frequencies of the filters were 0.1 MHz for the high pass and 3 MHz for the low pass. This device was sync to a digital oscilloscope (DPO 7054, Tektronix, WA, USA) in order to visualize and acquire the signals. The signals (record length 10k) from the transducer acting as receptor were amplified (40 – 60 dB), averaged (16 samples), digitalized (10 MS/s), transmitted to a PC and stored for further analysis.

Ultrasonic measurements

The transmitter and the receiver are embedded in a U-shaped holder facing each other at a distance of 30 to 50 mm depending on the center frequency of the transducers. The sample is located in between them at a slot which assures normal incidence. The received signal that has been transmitted through the sample and the air gaps is stored and the fast Fourier transform applied. Then, the transmission coefficient spectrum is calculated using a blank measurement as calibration. This process is repeated for each pair of transducers with the purpose of covering a wider frequency range.

Cycling experiments

A commercial charger (VLE8, Velleman, Belgium) was used to charge and discharge the battery cells. All the cycles were carried out with a current of C/2 at room temperature. After reaching each voltage point considered, the battery cell was put at rest no less than 15 minutes in order to stabilize it.

Thickness measurements

A micrometer (±0.01 mm, Mitutoyo, Kawasaki, Japan) was used to measure the thickness of the samples at 4 different points prior to the ultrasonic measurements. Due to the different designs within the set of samples considered in this study, the measured points were taken avoiding edges (the thickness of the sample is not constant through the whole cell) and other irregularities.

QUANTIFICATION AND STATISTICAL ANALYSIS

All data are expressed as mean ± SD as indicated on the appropriate figure legends. Numpy Python package was used for these statistical analysis.